Hindawi
Advances in Civil Engineering
Volume 2024, Article ID 2560804, 12 pages
https://doi.org/10.1155/2024/2560804

Research Article

Experimental Study on Mechanical Properties of CFRP-Confined Concrete Columns under Continuous Semi-Submergence of Sulfate

Mingxi Cai,[1] Lijun Shao,[1] Jiawei Zhang,[2] Kaijin Xu,[1] Jie Zhang,[1] and Penggang Li[1]

[1]*Lanzhou Nonferrous Metallurgical Design and Research Institute Industrial Design and Research Institute, Lanzhou, China*
[2]*School of Civil Engineering, Lanzhou Jiaotong University, Lanzhou 730070, China*

Correspondence should be addressed to Jiawei Zhang; zhangjd@mail.lzjtu.cn

Received 31 October 2023; Revised 22 February 2024; Accepted 27 March 2024; Published 15 April 2024

Academic Editor: Bang Yeon Lee

To investigate the mechanical properties of carbon-fiber-reinforced-polymer (CFRP)-restrained concrete in a saline soil environment, the degradation of the mechanical properties of CFRP-restrained concrete columns under the effect of continuous sulfate semisoak erosion is investigated based on sulfate continuous semisoak erosion, and unrestrained concrete columns with the same specifications are used in comparison tests. The results show that the strength, stiffness, and ductility of both plain concrete columns and CFRP-confined concrete columns first increase and then decrease after the continuous semi-submersion erosion by sulfate; compared with plain concrete columns, the decline rates of strength and stiffness of CFRP-confined concrete columns are significantly lower, and the CFRP demonstrates a certain protective effect on the core concrete. Through a regression analysis of experimental data, strength and ultimate strain models of CFRP-confined concrete columns under the continuous semi-submergence of sulfate are proposed based on the existing ultimate strength and ultimate strain models of CFRP-confined ordinary concrete columns, and a stress–strain model of CFRP-confined concrete columns under the continuous semi-submergence of sulfate is established. Based on a comparison with experimental data, the model prediction curves indicate good agreement with the experimental curves and can therefore provide a theoretical basis and practical reference for CFRP-reinforced semi-submerged concrete in saline soil areas.

1. Introduction

Fiber-reinforced polymer (FRPs) composites have been widely used in civil engineering structural reinforcement owing to their advantages of lightweight, high strength, high durability, and easy processing [1–3]. Among the reinforcement and strengthening methods for concrete columns or bridge piers, FRP wrapping is the most convenient and concise approach. FRP wrapping is used to repair and strengthen reinforced concrete columns or piers because it can effectively improve the bearing capacity and ductility of the members and prevent the longitudinal reinforcement from crimping in reinforced concrete members. Meanwhile, the chemical inertness of FRP can effectively reduce the erosion of the concrete matrix by sulfate [4–7].

FRP-restrained concrete columns have been investigated extensively, and many useful conclusions and theoretical models have been obtained. A study [8] showed that short columns restrained by two-layer CFRP wrapping increased the axial compressive strength to 150% of the unconfined strength and the strain value by approximately 615%. The one-layer CFRP restraint was enhanced, and the strain value increased by 200%. However, the increase in compressive strength was less significant, i.e., only approximately 75%. Experiments were performed in previous studies [9–16] to establish mechanical models of FRP-constrained concrete columns based on a force analysis between concrete and FRPs; subsequently, the mechanical behavior of FRP-constrained concrete columns was predicted. However, most of these models do not consider the effect of corrosive ions on the concrete matrix, which is the main factor that affects the durability of concrete structures.

The durability of FRP-constrained concrete columns has been investigated extensively. Freeze–thaw cycles, dry and wet cycles, and salt erosion degrade the mechanical

properties of FRP-constrained concrete members to varying degrees [17–23]. Kshirsagar et al. [24] investigated the durability of concrete bridge piers wrapped with FRPs. The durability of concrete piers was investigated using wet and dry cycles in the temperature range of −29 to 49°C and a relative humidity of 100%. Approximately 17 freeze–thaw cycles were performed, and a 2.7% decrease in compressive strength was observed. Saenz and Pantelides [25] evaluated concrete cylinders wrapped with CFRP under various environmental conditions (internal, external, and freeze–thaw cycles in salt water) and discovered a slight decrease in the axial strength, axial strain, and radial strain of the specimens. Micelli and Myers [26] showed that the ultimate strength of CFRP-coated cylinders immersed in a sodium chloride solution did not decrease significantly. Meanwhile, Harichandran et al. [27] evaluated CFRP-coated concrete cylinders for 300 wet and dry cycles and discovered that they did not significantly affect the compressive strength.

Salt erosion degrades the mechanical properties of CFRP-confined concrete columns [28–33], and the ultimate bearing capacity of the bonded interface decreases significantly with the extension of the erosion time. Concrete sulfate erosion is one of the most complex and hazardous factors affecting environmental water erosion. Zhou et al. [34] investigated the mechanical properties of FRP-confined concrete columns under the effect of sulfate erosion. They discovered that as the sulfate erosion time increased, the bearing capacity of FRP-confined concrete columns first increased slightly and then began to decrease considerably.

In practical engineering, it is not common for FRP-constrained concrete and concrete columns to be fully immersed in a sulfate environment. For concrete columns under semi-submersion, sulfate transport is primarily capillary adsorption and the "wick effect," which causes the region above the liquid surface to deteriorate more severely, whereas the region below the liquid surface is relatively intact. In Western China, numerous types of saline soils exist, and the corrosion of concrete columns or piers semiburied in saline soils is severe. Although the load-bearing capacity and ductility of concrete columns can be improved using CFRP winding reinforcement, the relevant theory is not sufficiently mature. Therefore, the mechanical properties of CFRP-confined concrete columns under the effect of continuous semi-submergence of sulfate must be investigated.

In this study, the degradation of the mechanical properties of CFRP-confined concrete columns under the continuous semi-submergence of sulfate was investigated based on erosion tests of continuous semi-submergence of sulfate, and a stress–strain relationship model [35–38] applicable to CFRP-confined concrete columns under the continuous semi-submergence of sulfate in saline soil areas was established to provide a theoretical basis for the application of CFRP-confined concrete columns in saline soil areas.

2. Experimental Overview

2.1. Experimental Design. A total of 26 concrete columns measuring 150 mm in diameter and 300 mm in height were used for the test.

The specimens were separated equally into two groups, one for the erosion test of ordinary concrete cylinders under the continuous semisoaking of sulfate solution, and one for the erosion test of CFRP-confined concrete cylinders under the continuous semisoaking of sulfate solution. The test box was a 547 mm × 415 mm × 330 mm plastic box without a lid, the sulfate solution was 10% sodium sulfate solution, and the semisoaking height was one-third of the concrete column, i.e., 100 mm. The CFRP-constrained concrete column prior to concrete soaking must be polished. Two layers of CFRP were used to wrap and reinforce the concrete column, and the lap length was 150 mm. The specific test steps are shown in Figure 1, the test environment and method are shown in Figure 2, and the concrete column after the sulfate semisoak erosion is shown in Figure 3.

The specific test number and grouping are listed in Tables 1 and 2, respectively, where CU indicates the unrestrained concrete specimen, CA the CFRP-constrained concrete cylinder, and H semisoaking. The number in front of "-" indicates the erosion time, and the number after that indicates the specimen number under the same conditions, e.g., CAH60-1 indicates CFRP-confined concrete cylinders subjected to sulfate semi-immersion for 60 days for specimen numbered 1. The impregnating rubber parameters are shown in Table 3, and the concrete ratio is shown in Table 4.

2.2. Axial Pressure Testing. The tests were performed based on the relevant provisions of the Standard on Test Methods for Concrete Structures (GB50152-92). A DH3816 static test strain gauge was used to measure the strain of the specimens when they were compressed. The test setup is illustrated in Figure 4.

3. Experimental Results and Analysis

3.1. Strength–Strain Variation Law of Ordinary Concrete Cylinders under Continuous Semi-Submergence of Sulfate. The variation pattern of the ultimate bearing capacity of plain concrete columns with the number of days of erosion under the continuous semisoaking of Na_2SO_4 solution is shown in Figure 5 and Table 5. The ultimate bearing capacity increased and then decreased as the number of erosion days increased. At 60 days of erosion, the strength was 47.71 MPa, the strength retention rate was 134.6%, and the strength increased by 34.6% relative to the natural environment. At 240 days of erosion, the strength was 26.52 MPa, the strength retention rate was 74.8%, and the strength decreased by 25.2% relative to the natural environment. At the early stage of erosion, the Na_2SO_4 solution reacted with the hydration products of concrete to generate gypsum and calcium alumina to fill the inherent pores of concrete, rendering the original concrete denser, at which time the ultimate bearing capacity and strength of concrete increased significantly. As the erosion age increased, the amounts of gypsum and calcium alumina continued to increase, and the concrete expanded internally, resulting in the loose spalling of concrete on the external surface and the appearance of microcracks. At this time, sulfate ions were more likely to enter the concrete interior, erosion products continued to accumulate,

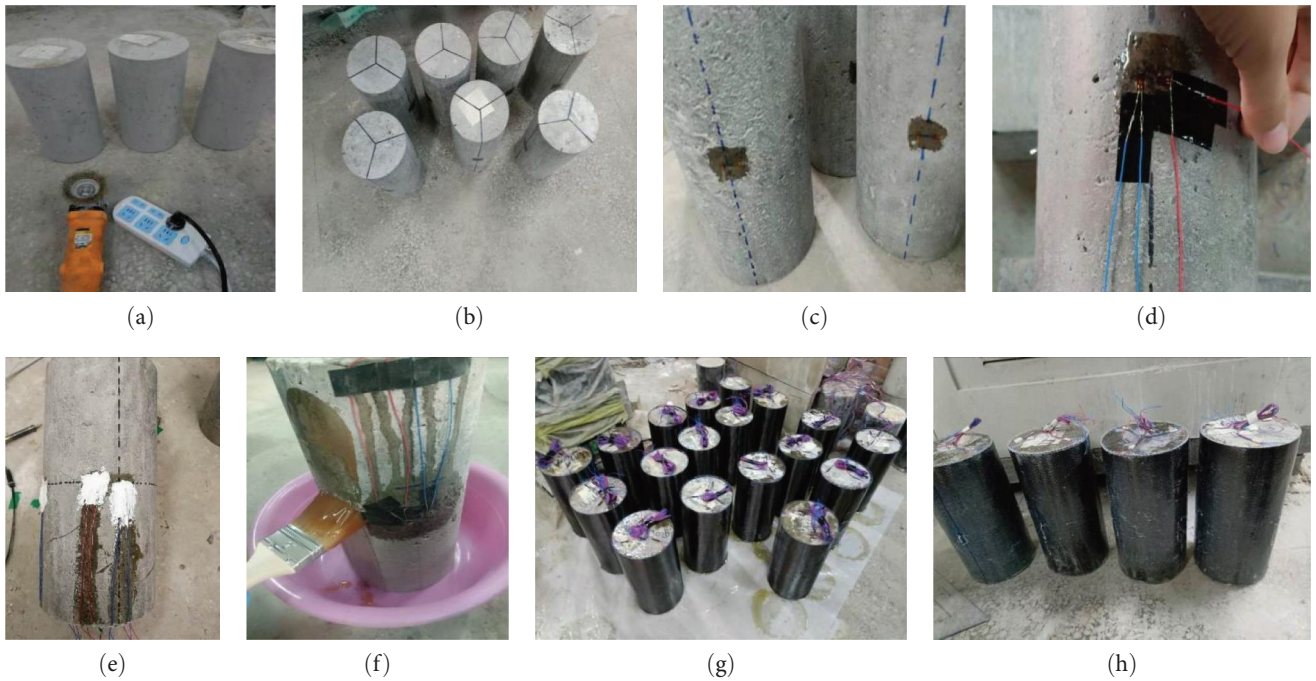

Figure 1: Test procedure: (a) polishing, (b) positioning, (c) sticking strain gauge, (d) connecting, (e) isolating, (f) applying dipping rubber primer, (g) pasting CFRP, and (h) pasting strain gauge on CFRP cloth.

Figure 2: Continuous half-immersion test of sulfate.

and the deterioration degree intensifies, resulting in a rapid decline in the bearing capacity and strength.

3.2. Stress–Strain Curves of Plain Concrete Cylinders under Continuous Semi-Submergence of Sulfate. The cylindrical stress–strain curve of plain concrete under the continuous semi-submersion of Na_2SO_4 solution is presented in Figure 6. As shown, the curve characteristics were similar to those under a natural environment. Three segments were observed: rising, parabola, and falling segments. At 60 days of erosion, the strength and strain were at their peak, with a maximum axial strain of 3.106×10^{-3} and a transverse strain of 2.789×10^{-3}. Compared with the natural environment, the axial and traverse strains were increased by 13.35% and 3.68%, respectively. At 240 days of erosion, the axial and traverse strains were 1.487×10^{-3} and 1.079×10^{-3}. Compared with the natural environment, the axial and traverse strains were reduced by 45.74% and 59.89%, respectively. At 60 days of erosion, the slope was the largest compared with the other erosion ages, which indicates that the stiffness was the highest at this time. As the age of erosion increased, the slope decreased, and the strength and strain decreased significantly, indicating that the strength, stiffness, and ductility of the Na_2SO_4 solution after continuous semi-submerged erosion first increased and then decreased.

3.3. Strength Variation of CFRP-Confined Concrete Cylinders. The test results of CFRP-constrained plain concrete cylinders under the continuous semisoaking of Na_2SO_4 solution are presented in Table 6. To present the effect of the continuous semisoaking of sulfate on the mechanical properties of the CFRP-constrained plain concrete cylinders more clearly, the ultimate strain ratio $\varepsilon_{cut}/\varepsilon_{cu0}$ is introduced herein. In fact, it can directly reflect the axial strain of CFRP-constrained plain concrete cylinders at different erosion ages compared with that of unconfined plain concrete cylinders.

As shown in Table 6 and Figure 7, the ultimate bearing capacity and compressive strength of the CFRP-confined

Figure 3: Concrete column corroded under continuous half-immersion of sulfate.

Table 1: Specimen grouping and numbering.

Test groups	Specimen number	Testing environment	Immersion age (days)	Number of CFRP binding layers	Number of specimens
1	CA0	Natural environment	0	2	3
2	CAH60	Continuous semisoaking	60	2	3
3	CAH90	Continuous semisoaking	90	2	3
4	CAH120	Continuous semisoaking	120	2	3
5	CAH180	Continuous semisoaking	180	2	3
6	CAH240	Continuous semisoaking	240	2	3

Table 2: Specimen grouping and numbering.

Test groups	Specimen number	Testing environment	Immersion age (days)	Number of CFRP binding layers	Number of specimens
1	CU0	Natural environment	0	0	3
2	CUH60	Continuous semisoaking	60	0	3
3	CUH90	Continuous semisoaking	90	0	3
4	CUH120	Continuous semisoaking	120	0	3
5	CUH180	Continuous semisoaking	180	0	3
6	CUH240	Continuous semisoaking	240	0	3

Table 3: Performance parameters of carbon fiber-reinforced polymer (CFRP) and carbon fiber impregnant.

CFRP property		Impregnant property	
Tensile strength (MPa)	≥3,400	Tensile strength (MPa)	≥38
Nominal thickness (mm)	0.167	Flexural strength (MPa)	≥50
Elongation (%)	≥1.6	Elongation (%)	≥1.5
Mass per unit area ($g.m^{-2}$)	300	Compressive strength (MPa)	≥70
Modulus of elasticity in tension (MPa)	$\geq 2.3 \times 10^5$	Modulus of elasticity in tension (MPa)	≥2,400

Table 4: Concrete mix ratio.

Water (kg/m^3)	Cement (kg/m^3)	Fly ash (kg/m^3)	Sand washing (kg/m^3)	Gravel (kg/m^3)	Water reducing agent (kg/m^3)	Sand and stone (%)	Sand water (%)
114	269	59	1,043	927	8.2	15	5

Figure 4: Diagram of test device.

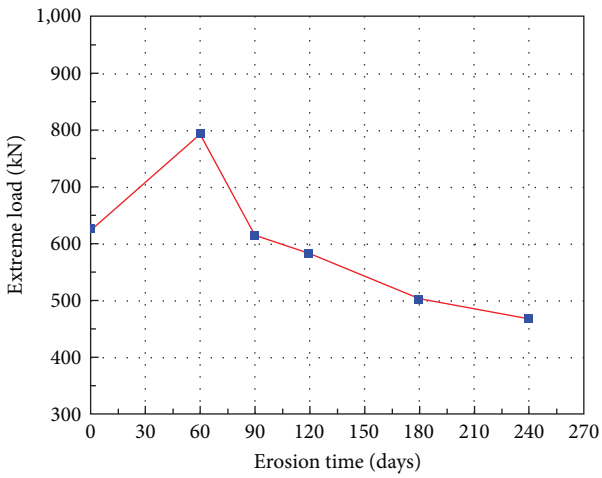

Figure 5: Relationship between ultimate bearing capacity of ordinary concrete cylinder and erosion time under continuous half-immersion in Na_2SO_4 solution.

plain concrete under the continuous semisoaking of Na_2SO_4 solution first increased and then decreased as the erosion time increased. At 90 days of erosion, the compressive strength was 106.74 MPa and the strength retention rate was 105.4%, which was an increase of 5.4% relative to the strength after CFRP restraint in the natural environment; at 240 days of erosion, the compressive strength was 98.76 MPa and the strength retention rate was 97.52%, which was a decrease by 2.48% relative to the strength after CFRP restraint in the natural environment. Based on the data, the magnitude of the strength decrease was controlled within 6%. Furthermore, the strength decrease at the same age was significantly less than that of ordinary concrete cylinders, such as unrestrained concrete cylinders, which indicated a strength decrease of approximately 26.36% after 240 days of erosion, whereas the ordinary concrete cylinders wrapped by CFRP indicated a strength decrease of only approximately 2.48%. CFRP is highly durable in a sulfate environment, and its mechanical properties do not decrease significantly as the erosion time increases. Meanwhile, the concrete columns wrapped with CFRP effectively prevented sulfate ions from entering the concrete, thereby protecting the concrete.

The stress–strain curve of CFRP-confined ordinary concrete under the continuous semisoaking of Na_2SO_4 solution is presented in Figure 8. As shown, the stress–strain curve of the CFRP-confined ordinary concrete exhibited a trilinear segment. However, compared with the ordinary concrete cylindrical stress–strain curve, it exhibited a descending segment into a rising straight segment after the parabolic segment. The change patterns of the peak stress and ultimate strain with erosion time were similar to those of ordinary concrete columns, both of which indicated a slight increase followed by a decrease as the erosion time increased. At 90 days of erosion, both the strength and strain were at their peak, with a maximum axial strain of 17.89×10^{-3} and a transverse strain of 15.509×10^{-3}, respectively, which corresponded to increases by 18.24% and 43.77% compared with those in the natural environment, respectively. At 240 days of erosion, the axial and traverse strains were 13.202×10^{-3} and 9.911×10^{-3}, respectively, which were 12.74% and 8.12% lower than those of the natural environment, respectively. At 90 days of erosion, the slope was the largest compared with those of the other erosion ages, which indicates that the stiffness was the highest at this time. As the erosion age increased, the slope continued to decrease, and the strength and strain decrease significantly, indicating that the strength, stiffness, and ductility of the CFRP-confined plain concrete columns first increased and then decreased after the erosion by the continuous semisoaking of the Na_2SO_4 solution. This is similar to the changing pattern of unconfined concrete columns under the continuous semisoaking of sulfate, except that the CFRP prevented the erosion of sulfate ions, which decreased the strength and stiffness of the specimens for a longer time and to a lower degree.

4. Stress–Strain Model of CFRP-Confined Concrete Cylinder

4.1. Effect of Sulfate Action on Cylindrical Strength and Ultimate Strain of Plain Concrete. The mechanical properties of concrete cylinders further degraded as the immersion time increased. In this study, an influence function associated with the soaking time was introduced to reflect the effect of sulfate semisoaking on the concrete strength and its corresponding compressive strain.

4.1.1. Strength Retention Rate of Concrete. The concrete strength retention rate is expressed as follows:

$$R_{f1} = \frac{f'_{ct}}{f'_{c0}}, \tag{1}$$

where R_{f1} is the concrete strength retention rate, f'_{c0} is the for ease of presentation later, replace f'_c with f'_{c0}, and f'_{ct} is the compressive strength of concrete at each age of erosion.

The relationship between the compressive strength of concrete and the time of sulfate attack can be expressed as follows:

$$\frac{f'_{ct}}{f'_{c0}} = R_{f1} = \gamma_{f1}(t). \tag{2}$$

By fitting the curve of the compressive strength of concrete with the time of continuous sulfate immersion. As

Table 5: Changes in strength and strain of ordinary concrete cylinders under continuous half-immersion in Na_2SO_4 solution.

Specimen number	F (kN)	$f_{cut'}$ (MPa)	$F_{cut'}$, m (MPa)	ε_{cut} ($\times 10^{-6}$)	ε_l ($\times 10^{-6}$)	R (%)	R_m (%)
CU0-1	627.61	35.53		2,810	2,604		
CU0-2	653.18	36.98	35.45	2,719	2,707	100	100
CU0-3	597.54	33.83		2,692	2,759		
CUH60-1	814.17	46.09	44.88	3,045	2,803	130.01	126.6
CUH60-2	771.35	43.67		3,106	2,789	123.19	
CUH90-1	617.71	34.97	34.73	2,644	2,231	98.65	97.96
CUH90-2	608.98	34.48		2,498	2,178	97.26	
CUH120-1	568.51	32.19	32.89	2,276	1,904	90.80	92.79
CUH120-2	593.50	33.60		2,068	1,876	94.79	
CUH180-1	500.35	28.33	28.43	1,788	1,468	79.91	80.18
CUH180-2	503.78	28.52		1,690	1,404	80.46	
CUH240-1	475.67	26.93	26.52	1,456	1,192	75.97	74.80
CUH240-2	461.08	26.11		1,487	1,079	73.64	

Note: F is the ultimate bearing capacity, $f_{cut'}$ is the compressive strength of specimens, $f_{cut'}$, m is the average compressive strength of specimens, ε_{cut} is the axial strain, ε_l is the lateral strain, R is the strength retention rate, and R_m is the average strength retention rate.

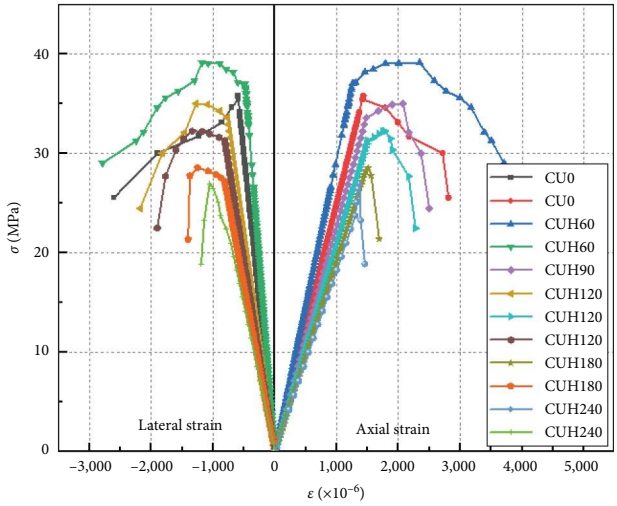

Figure 6: Stress–strain curve of ordinary concrete cylinder under continuous half-immersion in Na_2SO_4 solution.

shown in Figure 9, the time effect function can be expressed as follows:

$$\gamma_{f1}(t) = 1 + 0.00032t - 0.0000062t^2. \tag{3}$$

4.1.2. Strain Retention Rate. Similar to the expression of concrete strength, the concrete compressive strain retention rate is expressed as follows:

$$R_{\varepsilon 1} = \frac{\varepsilon'_{ct}}{\varepsilon'_{c0}}, \tag{4}$$

where $R_{\varepsilon 1}$ is the concrete strain retention rate; ε'_{c0} is the for sake of clarity in the later expressions, ε'_{c0} is used as a substitute for the compressive strain corresponding to an unconfined concrete compressive strength f'_c at the standard curing age (28 days) ε'_c; ε'_{ct} is the compressive strength of concrete at each f'_{ct}.

The relationship between ε'_{ct} and t can be expressed as follows:

$$\frac{\varepsilon'_{ct}}{\varepsilon'_{c0}} = R_{\varepsilon 1} = \gamma_{\varepsilon 1}(t). \tag{5}$$

Meanwhile, $\gamma_{\varepsilon 1}(t)$ as a function of time can be obtained by fitting the compressive strength of concrete compressive strength to the sulfate continuous immersion action time variation curve, as shown in Figure 10, as follows:

$$\gamma_{\varepsilon 1}(t) = 1 - 0.000066t - 0.0000086t^2. \tag{6}$$

4.2. Limit Strength and Strain Model for CFRP-Confined Plain Concrete Columns under Sulfate Action

4.2.1. Strength Model. Herein, the expression form of the strength model of Toutanji [39] is used to analyze the stress–strain relationship of CFRP-confined concrete cylinders. The ultimate strength of CFRP-confined plain concrete cylinders under sulfate immersion can be expressed as follows:

$$\frac{f'_{cut}}{f'_{ct}} = 1 + k_1\left(\frac{f_{lu}}{f'_{ct}}\right), \tag{7}$$

where f'_{cut} is the compressive strength of CFRP-confined concrete at immersion time t under the continuous semisubmersion of sulfate; f'_{ct} is the compressive strength of ordinary concrete cylinders under the continuous semisoaking of sulfate with soaking time t; k_1 is the constant to be determined, where $k_1 = 4.38$ was obtained in this study by fitting the experimental data. Meanwhile, the effective lateral restraint strength, f_{lu}, is calculated as follows:

Table 6: Strength variation of deteriorated concrete confined by CFRP under two stages.

Specimen number	F (kN)	$f_{cut'}$ (MPa)	$f_{cut'}$, m (MPa)	ε_{cut} ($\times 10^{-6}$)	ε_l ($\times 10^{-6}$)	$\varepsilon_{cut}/\varepsilon_{cu0}$	R (%)	R_m (%)
CA0-1	1,762.61	99.79		15,403	11,205	5.62		
CA0-2	1,840.62	104.21	101.27	15,007	10,567	5.47	—	100
CA0-3	1,762.61	99.79		14,982	10,589	5.46		
CAH60-1	1,876.30	106.23	106.48	16,032	14,302	5.85	104.90	105.15
CAH60-2	1,885.22	106.74		15,543	13,908	5.67	105.40	
CAH90-1	1,892.09	107.12	106.74	17,890	15,509	6.53	105.78	105.4
CAH90-2	1,878.43	106.35		18,032	15,231	6.58	105.02	
CAH120-1	1,842.87	104.34	104.05	15,602	11,708	5.69	103.03	102.745
CAH120-2	1,832.62	103.76		15,409	12,032	5.62	102.46	
CAH180-1	1,842.14	104.30	102.18	14,992	12,389	5.47	102.99	100.9
CAH180-2	1,767.22	100.06		15,202	11,809	5.55	98.81	
CAH240-1	1,728.75	97.88	98.76	13,202	9,911	4.82	96.65	97.52
CAH240-2	1,759.88	99.64		14,283	8,901	5.21	98.39	

Note. F is the ultimate bearing capacity, $f_{cut'}$ is the compressive strength of specimens, $f_{cut'}$, m is the average compressive strength of specimens, ε_{cut} is the axial strain, ε_l is the lateral strain, R is the strength retention rate, and R_m is the average strength retention rate.

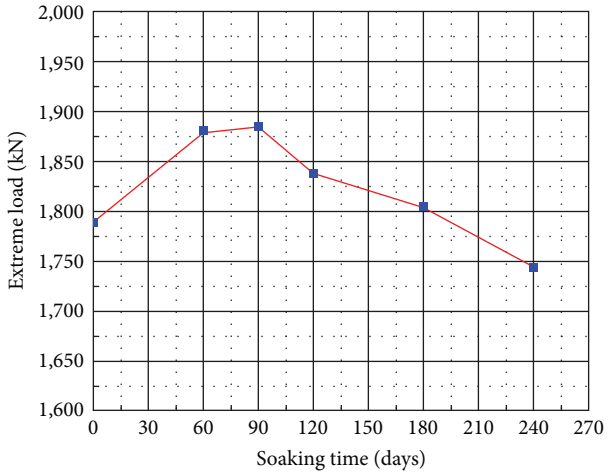

Figure 7: Relationship between ultimate bearing capacity and erosion time of CFRP-constrained ordinary concrete.

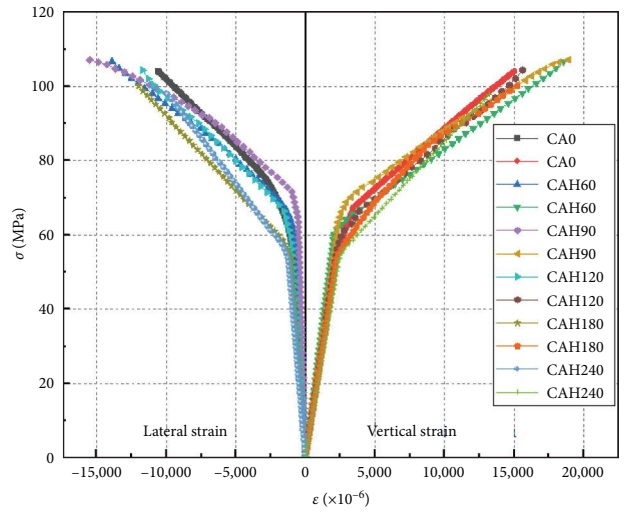

Figure 8: Stress–strain curve of CFRP-confined plain concrete under continuous semi-submersion of Na_2SO_4 solution.

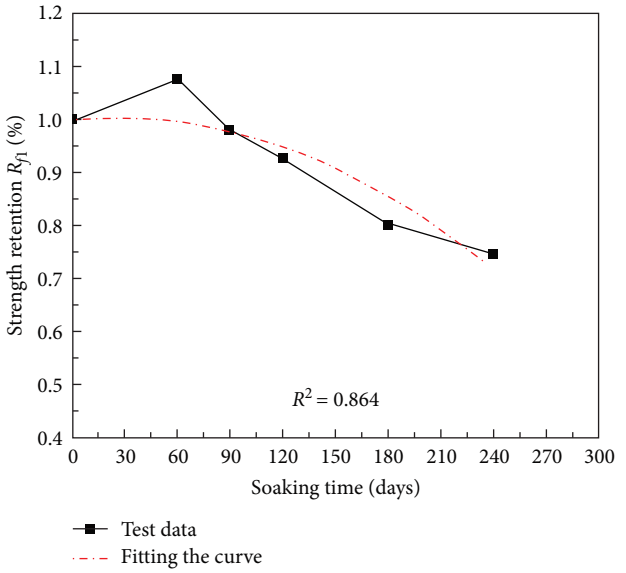

Figure 9: Curve of compressive strength of concrete vs. immersion time.

$$f_{lu} = \frac{2nt_f f_{fu}}{d}, \tag{8}$$

where f_{fu} is the ultimate tensile strength of the CFRP material, t_f the thickness of the CFRP material, and d the diameter of the specimen.

After the concrete cylinders were pasted with CFRP, the rate of strength reduction of CFRP-confined concrete cylinders under the semisoaking of sulfate was discovered to be significantly lower than that of ordinary concrete cylinders because the CFRP offers better corrosion resistance and can effectively prevent sulfate ions from entering the concrete interior. The strength retention rate of CFRP-confined concrete cylinders under sulfate immersion, R_{f2} can be expressed as follows: By fitting the curve of R_{f2} changing with erosion

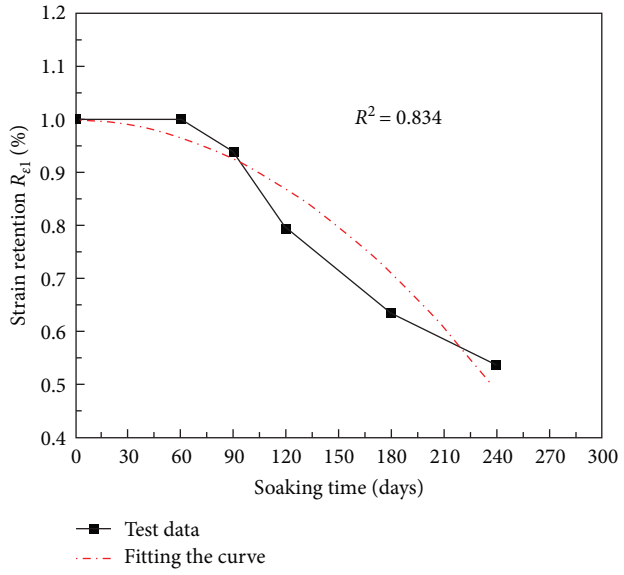

Figure 10: Limit strain vs. immersion time curve.

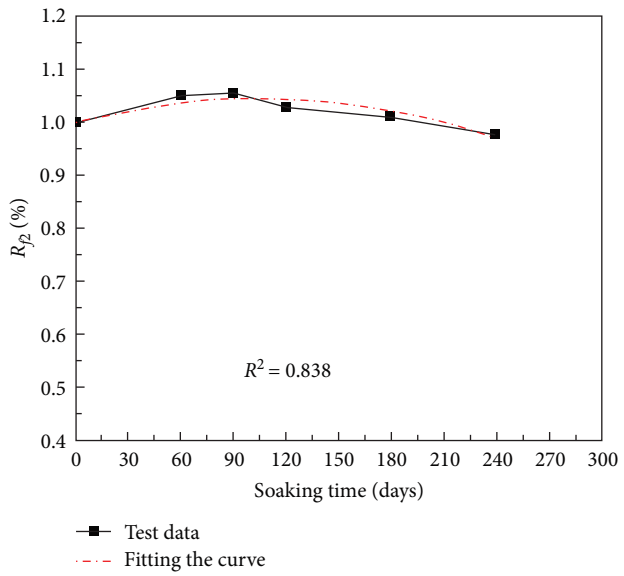

Figure 11: Strength vs. immersion time curve.

time, as shown in Figure 11, it can be obtained that $y_{f2}(t)$. The calculation expression for Equation (10) is given as follows:

$$R_{f2} = \frac{f'_{cuT}}{f'_{cu0}} = \gamma_{f2}(t), \tag{9}$$

$$\gamma_{f2}(t) = 1 + 0.00084t - 0.000004t^2. \tag{10}$$

Substituting Equation (9) into Equation (7) yields an expression for the cylindrical strength model of CFRP-confined concrete under the action of sulfate, as follows:

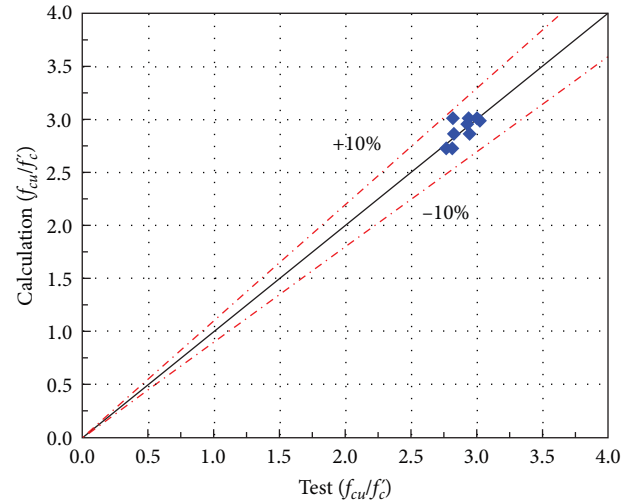

Figure 12: Comparison between predicted and evaluated values of the proposed strength model.

$$\frac{f'_{cut}}{f'_{c0}} = R_{f2} + 4.38\left(\frac{f_{lu}}{f'_{c0}}\right). \tag{11}$$

Figure 12 shows a comparison between the predicted and evaluated values of the proposed strength model. As shown, the proposed cylindrical strength model of CFRP-confined concrete under sulfate immersion agreed well with the test results, with both positive and negative deviations of less than 10%. Furthermore, the proposed strength model demonstrated high prediction accuracy.

4.2.2. Strain Model. In this study, the expression form of the De Lorenzis model [40] was used to analyze the CFRP-constrained concrete cylindrical strain, and the ultimate strain model for CFRP-constrained plain concrete cylinders under sulfate immersion can be expressed as follows:

$$\frac{\varepsilon_{cut}}{\varepsilon'_{ct}} = 1 + k_2\left(\frac{f_{lu}}{f'_{ct}}\right)E_l^{-0.148}, \tag{12}$$

where ε_{cut} is the ultimate compressive strain of CFRP-confined concrete at immersion time t under the continuous semi-submersion of sulfate; ε'_{ct} is the ultimate compressive strain of ordinary concrete cylinders under the continuous semisoaking of sulfate with soaking time t; k_2 is the constant to be determined, where $k_2 = 30.6$ was obtained in this study by fitting the experimental data.

After the concrete cylinders were pasted with CFRP, the rate of strain decrease in the CFRP-constrained concrete cylinders under the semisoaking of sulfate was significantly lower than that of ordinary concrete cylinders because the CFRP offers better corrosion resistance and can effectively prevent sulfate ions from entering the concrete interior. The ultimate strain retention rate of CFRP-confined concrete cylinders under sulfate immersion can be expressed as follows:

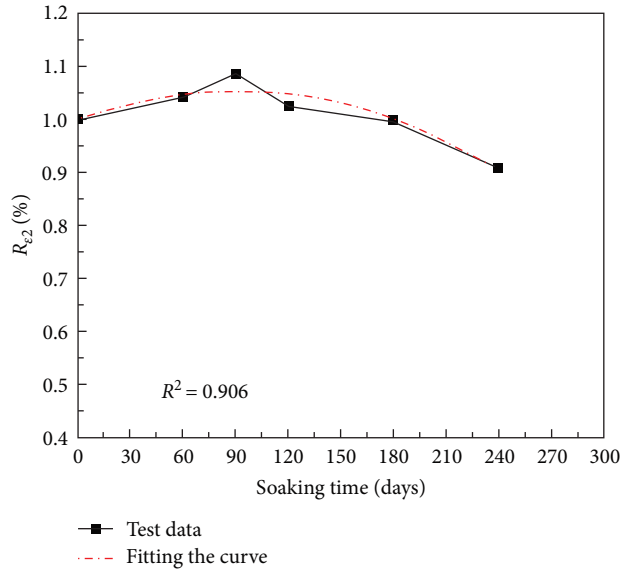

Figure 13: Strength vs. immersion time curve.

$$R_{\varepsilon 2} = \frac{\varepsilon_{cut}}{\varepsilon_{cu0}} = \gamma_{\varepsilon 2}(t). \tag{13}$$

The calculated expression for $\gamma_{\varepsilon 2}(t)$ can be obtained by fitting the variation curve of $R_{\varepsilon 2}$ with erosion time, as shown in Figure 13:

$$\gamma_{\varepsilon 2}(t) = 1 + 0.00121t - 0.0000067t^2. \tag{14}$$

Substituting Equations (13) and (9) into Equation (12) yields the expression for the ultimate strain retention rate, as follows:

$$\frac{\varepsilon_{cut}}{\varepsilon_c'} = 0.4R_{\varepsilon 2} + 30.6 \cdot \frac{R_{\varepsilon 2}}{R_{f2}} \left(\frac{f_{lu}}{f_{c0}'}\right) E_l^{-0.148}. \tag{15}$$

Figure 14 shows a comparison between the predicted and experimental values of the proposed strain model. As shown, the proposed cylindrical strain model for CFRP-confined concrete under the semisoaking of sulfate agreed well with the experimental results, and the positive and negative deviations were less than 20%. Hence, the proposed strain model offers high prediction accuracy.

4.2.3. Cylindrical Stress–strain Model for Proposed CFRP-Constrained Concrete. The analysis of the stress–strain relationship curve for CFRP-constrained concrete (based on Figure 8) shows that the curve can be partitioned into two segments, i.e., the segment indicating nonlinear growth before the stress reaches the turning point and the linear growth segment thereafter. For the first segment of the curve prior to the turning point, the curve form Lam and Teng [13] model was used in this study for analysis, and the relevant expressions are as follows:

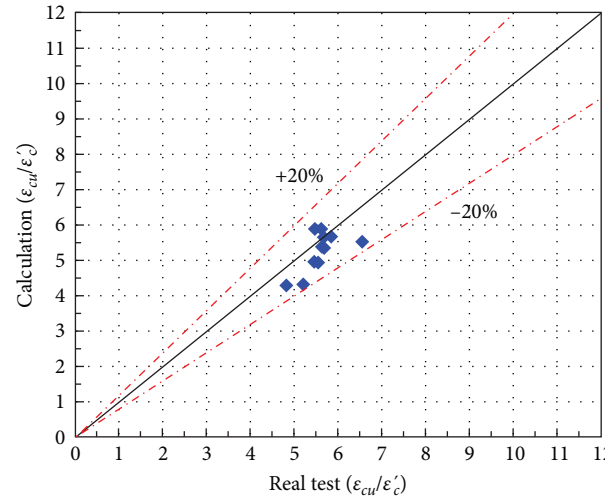

Figure 14: Comparison between predicted and evaluated values of the proposed strain model.

$$\sigma_c = E_c\varepsilon_c - \frac{(E_c - E_2)^2}{4f_{co}'}\varepsilon_c^2, \tag{16}$$

$$\sigma_t = E_c\varepsilon_t - \frac{(E_c - E_2)^2}{4f_{co}'}\varepsilon_t^2, \tag{17}$$

$$\varepsilon_t = \frac{2f_c'}{E_c - E_2}, \tag{18}$$

where σ_c and ε_c of the stress and strain in the restrained concrete, respectively, σ_t and ε_t are the stress and strain at the turning point, respectively, E_c is the modulus of elasticity of unconfined concrete, and f_{cu}' and ε_{cu} denote the ultimate strength and strain of the restrained concrete at the time of damage, respectively. The slope of the straight line segment from the turning point to the limit breaking point is denoted as E_2.

The slope of the second segment of the line is expressed as follows:

$$E_2 = \frac{f_{cu}' - f_c'}{\varepsilon_{cu}}. \tag{19}$$

The complete stress–strain curve is obtained by substituting the obtained strength model and the ultimate strain model of the CFRP-confined plain concrete cylinder under the semisoaking of sulfate into the expressions of the first and second stages. Recommended models obtained cylindrical stress–strain curve of CFRP-confined concrete and the experimentally obtained stress–strain curve are shown in Figure 15. As shown, as the erosion time increased, the predicted and experimental values of the proposed model indicated better agreement. This is because the value of the intersection of the reverse extension line of the second segment of the curve with the longitudinal axis was greater than the compressive strength of concrete when it was restrained owing to the stronger restraint of the concrete when the

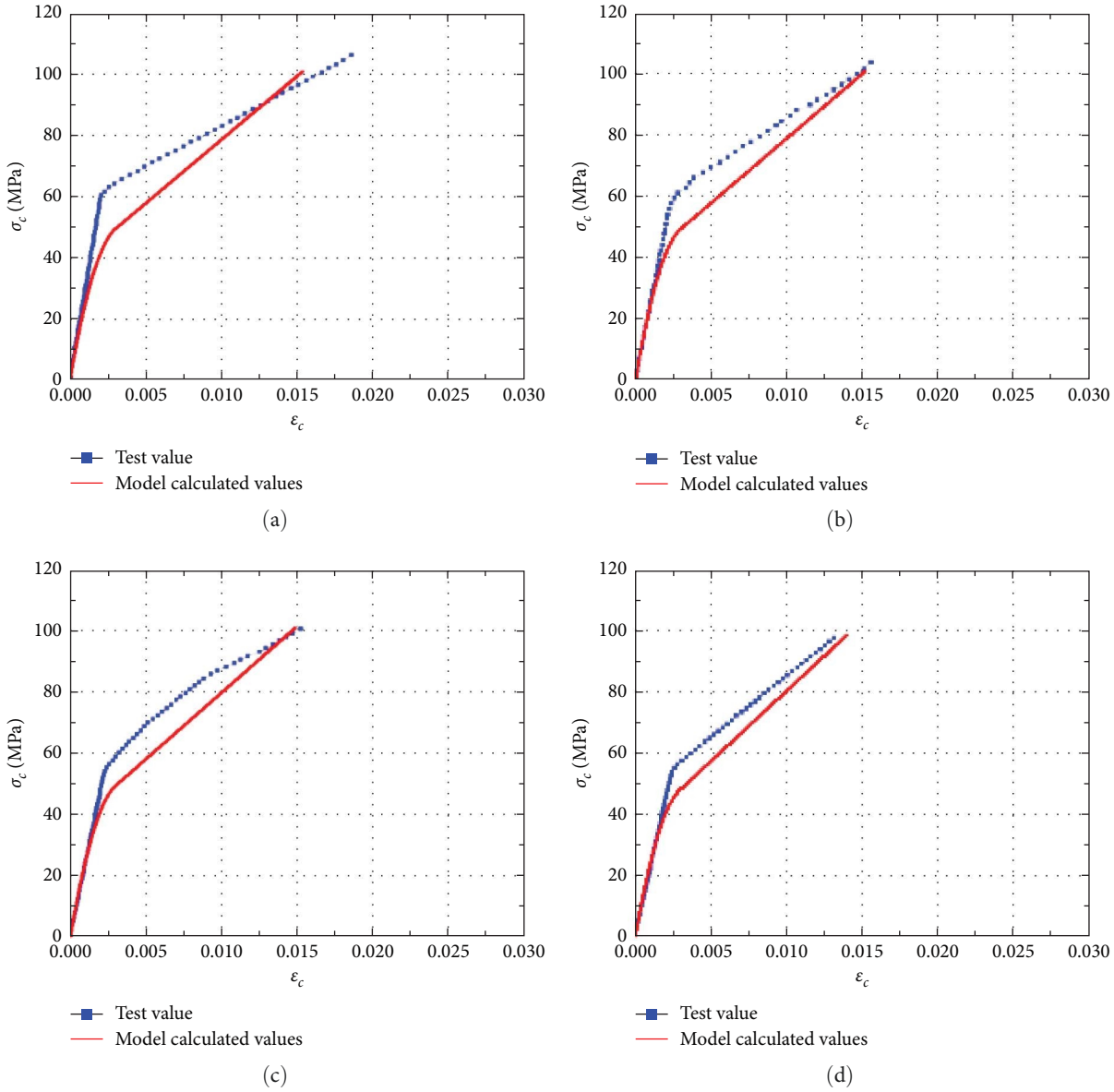

Figure 15: Comparison between predicted and experimental values of proposed model: (a) CAH60, (b) CAH120, (c) CAH180, and (d) CAH240.

number of CFRP-pasted layers was two, which we assumed as the compressive strength of the restrained concrete cylinder in the model calculation. Therefore, the stress at the inflection point was lower than the test value. As the erosion time increased, the concrete became damaged, and the restraint effect of CFRP on the concrete column diminished gradually, which caused the inflection point of the stress–strain curve to shift down. Meanwhile, the value of the intersection of the reverse extension line of the second curve and the longitudinal axis decreased and was similar to the strength of the restrained concrete column at the same erosion time, thereby resulting in a close match between the predicted and experimental values of the model.

5. Conclusion

(1) The strength, stiffness, and ductility of both plain concrete columns and CFRP-confined concrete columns first increased and then decreased after the continuous semisoaking erosion of sulfate; compared with the plain concrete columns, the rates of decrease of strength and stiffness of the CFRP-confined concrete columns were significantly lower, and CFRP exerted a certain protective effect on the core concrete.

(2) Based on the existing strength model of FRP-confined concrete columns and ultimate strain models, the compressive strength and ultimate strain models of

ordinary concrete columns and CFRP-confined ordinary concrete (deteriorated concrete) columns under the continuous semi-submergence of sulfate were obtained by fitting the experimental data.

(3) A stress–strain model for CFRP-confined concrete (deteriorated concrete) cylinders under the continuous semi-submergence of sulfate was developed, and the predicted curves matched well with the experimental curves.

Data Availability

All relevant data are within the paper. No additional data are available.

Conflicts of Interest

The authors declare that they have no conflicts of interest.

Acknowledgments

First of all, I would like to thank my supervisor, Prof. Jiawei Zhang, for his long-term care and teaching, from the selection of the thesis topic, the design of the experimental protocol, to the revision and successful completion of the thesis, all without the careful guidance of my mentor. I would like to thank Mr. Yanjin Xue from the Road and Bridge Laboratory for her continuous support and help in my experiments. I also thank Mr. Dajian Huang from the School of Materials Engineering for his great help in my microscopic experiments, and Mr. Jianchang Zhao, Mr. Bentian Yu, Ms. Manlin Huo, Ms. Fenqin Zhang, and Mr. Tingbin Liu from the School of Structural Engineering for their utmost help and guidance in deciding the experimental protocol and using the experimental instruments. In this work, financial support received from the National Natural Science Foundation of China (grant number 52068043), the Lanzhou Science and Technology Planning Project (grant number 2018-1-18), and the Lanzhou Talent Innovation and Entrepreneurship Project (grant number 2019-RC-78). We would like to thank Editage (https://www.editage.cn/) for English language editing.

References

[1] Y. J. Kim, M. Hossain, and J. Zhang, "A probabilistic investigation into deterioration of CFRP-concrete interface in aggressive environments," *Construction and Building Materials*, vol. 41, pp. 49–59, 2013.

[2] Y. J. Kim, M. Hossain, and Y. Chi, "Characteristics of CFRP-concrete interface subjected to cold region environments including three-dimensional topography," *Cold Regions Science and Technology*, vol. 67, no. 1-2, pp. 37–48, 2011.

[3] S. Nolan, M. Rossini, C. Knight, and A. Nanni, "New directions for reinforced concrete coastal structures," *Journal of Infrastructure Preservation and Resilience*, vol. 2, no. 1, 2021.

[4] ACI Committee 440, *Guide for the Design and Construction of Externally Bonded FRP Systems for Strengthening Concrete Structures*, American Concrete Institute, Farmington Hills, Michigan, 2002.

[5] Z. Tang, S. Yang, and H. Gao, "Comparison of uniaxial compressive damage of concrete under sulfate erosion and dry wet, freeze-thaw cycles," *Silicate Bulletin*, vol. 2, pp. 428–438, 2024.

[6] L. Shao, *Experimental Study on the Performance of CFRP Confined Concrete Cylinders Under Continuous Semi Immersion with Sulfate*, Lanzhou Jiaotong University, 2021.

[7] J. Zhang, L. Shao, S. Liu, F. Luo, Z. Yang, and R. Zhang, "Mechanical properties of CFRP constrained deteriorated concrete columns in sulfate environments," *Acta Materiae Compositae Sinica*, vol. 38, no. 3, pp. 966–978, 2021.

[8] M. S. Radhi, I. N. Gorgis, and M. S. Hassan, "Analytical analysis of design-oriented models for forecasting the performance of CFRP-confined corrosion-affected concrete columns," *Construction and Building Materials*, vol. 313, pp. 196–206, Article ID 125491, 2021.

[9] J. F. Berthet, E. Ferrier, and P. Hamelin, "Compressive behavior of concrete externally confined by composite jackets," *Construction and Building Materials*, vol. 20, no. 5, pp. 338–347, 2006.

[10] T. Jiang and J. G. Teng, "Analysis-oriented stress–strain models for FRP-confined concrete," *Engineering Structures*, vol. 29, no. 11, pp. 2968–2986, 2007.

[11] A. I. Karabinis and T. C. Rousakis, "Concrete confined by FRP material: a plasticity approach," *Engineering Structures*, vol. 24, no. 7, pp. 923–932, 2002.

[12] V. M. Karbhari and Y. Gao, "Composite jacketed concrete under uniaxial compression—verification of simple design equations," *Journal of Materials in Civil Engineering*, vol. 9, no. 4, pp. 185–193, 1997.

[13] L. Lam and J. G. Teng, "Design-oriented stress–strain model for FRP-confined concrete," *Construction and Building Materials*, vol. 17, no. 6-7, pp. 471–489, 2003.

[14] S. Matthys, H. Toutanji, and L. Taerwe, "Stress–strain behavior of large-scale circular columns confined with FRP composites," *Journal of Structural Engineering*, vol. 132, no. 1, pp. 123–133, 2006.

[15] Y.-F. Wu and Y.-W. Zhou, "Unified strength model based on Hoek–Brown failure criterion for circular and square concrete columns confined by FRP," *Journal of Composites for Construction*, vol. 14, no. 2, pp. 175–184, 2010.

[16] V. Yazici and M. N. S. Hadi, "Normalized confinement stiffness approach for modeling FRP-confined concrete," *Journal of Composites for Construction*, vol. 16, no. 5, pp. 520–528, 2012.

[17] I. Alachek, N. Reboul, and B. Jurkiewiez, "Bond strength's degradation of GFRP-concrete elements under aggressive exposure conditions," *Construction and Building Materials*, vol. 179, pp. 512–525, 2018.

[18] S. A. Hadigheh, R. J. Gravina, and S. T. Smith, "Effect of acid attack on FRP-to-concrete bonded interfaces," *Construction and Building Materials*, vol. 152, pp. 285–303, 2017.

[19] C. Tuakta and O. Büyüköztürk, "Deterioration of FRP/concrete bond system under variable moisture conditions quantified by fracture mechanics," *Composites Part B: Engineering*, vol. 42, no. 2, pp. 145–154, 2011.

[20] J. R. Cromwell, K. A. Harries, and B. M. Shahrooz, "Environmental durability of externally bonded FRP materials intended for repair of concrete structures," *Construction and Building Materials*, vol. 25, no. 5, pp. 2528–2539, 2011.

[21] M. A. G. Silva and H. Biscaia, "Degradation of bond between FRP and RC beams," *Composite Structures*, vol. 85, no. 2, pp. 164–174, 2008.

[22] M. Ekenel, J. Myers, and A. Khataukar, "Affect of environmental conditions during installation process on bond strength between

CFRP laminate and concrete substrate," in *3rd International Conference Composites in Construction*, pp. 397–404, Researchgate, Lyon, France, 2005.

[23] S. Wang and M. A. ElGawady, "Effects of hybrid water immersion, environmental exposures, and axial load on the mechanical properties of concrete filled epoxy-based glass fiber reinforced polymer tubes," *Construction and Building Materials*, vol. 194, pp. 311–321, 2019.

[24] S. Kshirsagar, R. Lopez-Anido, and R. K. Gupta, "Durability of fiber reinforced composite wrapping for the rehabilitation of concrete piers," in *Proceedings of the 1st conference on Durability of Fiber Reinforced Polymer (FRP) Composites for Construction (CDCC 1998)*, pp. 117–128, University of Sherbrooke, Sherbrooke, 1998.

[25] N. Saenz and C. P. Pantelides, "Short and medium term durability evaluation of FRP-confined circular concrete," *Journal of Composites for Construction*, vol. 10, no. 3, pp. 244–253, 2006.

[26] F. Micelli and J. J. Myers, "Durability of FRP-confined concrete," *Proceedings of the Institution of Civil Engineers—Construction Materials*, vol. 161, no. 4, pp. 173–185, 2008.

[27] R. S. Harichandran, M. I. Baiyasi, and G. Nossoni, "Freeze-thaw durability of concrete columns wrapped with FRP and subject to corrosionlike expansion," *Journal of Materials in Civil Engineering*, vol. 29, no. 1, 2017.

[28] M. N. Youssef, M. Q. Feng, and A. S. Mosallam, "Stress–strain model for concrete confined by FRP composites," *Composites Part B: Engineering*, vol. 38, no. 5-6, pp. 614–628, 2007.

[29] E. Vintzileou and E. Panagiotidou, "An empirical model for predicting the mechanical properties of FRP-confined concrete," *Construction and Building Materials*, vol. 22, no. 5, pp. 841–854, 2008.

[30] M. Z. Y. Ting, K. S. Wong, M. E. Rahman, and S. J. Meheron, "Deterioration of marine concrete exposed to wetting-drying action," *Journal of Cleaner Production*, vol. 278, Article ID 123383, 2021.

[31] E. Rozière, A. Loukili, R. El Hachem, and F. Grondin, "Durability of concrete exposed to leaching and external sulphate attacks," *Cement and Concrete Research*, vol. 39, no. 12, pp. 1188–1198, 2009.

[32] Z. Liu, X. N. Li, D. Deng, G. De Schutter, and L. Hou, "The role of $Ca(OH)_2$ in sulfate salt weathering of ordinary concrete," *Construction and Building Materials*, vol. 123, pp. 127–134, 2016.

[33] B. Mota, T. Matschei, and K. Scrivener, "The influence of sodium salts and gypsum on alite hydration," *Cement and Concrete Research*, vol. 75, pp. 53–65, 2015.

[34] Y. Zhou, M. Li, L. Sui, and F. Xing, "Effect of sulfate attack on the stress–strain relationship of FRP-confined concrete," *Construction and Building Materials*, vol. 110, pp. 235–250, 2016.

[35] F. E. Richart, A. Brandtzaeg, and R. L. Brown, *A Study of the Failure of Concrete Under Combined Compressive Stress*, University of Illinois, Engineering Experimental Station, Illinois, 1928.

[36] Z. Yan, C. P. Pantelides, and L. D. Reaveley, "Fiber-reinforced polymer jacketed and shape-modified compression members: II-model," *ACI Structural Journal*, vol. 103, pp. 894–903, 2006.

[37] L. Lam and J. G. Teng, "Strength models for fiber-reinforced plastic-confined concrete," *Journal of Structural Engineering*, vol. 128, no. 5, pp. 612–623, 2002.

[38] Y. Xiao and H. Wu, "Compressive behavior of concrete confined by carbon fiber composite jackets," *Journal of Materials in Civil Engineering*, vol. 12, no. 2, pp. 139–146, 2000.

[39] H. Toutanji, "Stress-strain characteristics of concrete columns externally confined with advanced fiber composite sheets," *Materials*, vol. 96, pp. 397–404, 1999.

[40] L. De Lorenzis and R. Tepfers, "Comparative study of models on confinement of concrete cylinders with fiber-reinforced polymer composites," *Journal of Composites for Construction*, vol. 7, pp. 219–237, 2003.